T-963

NMT
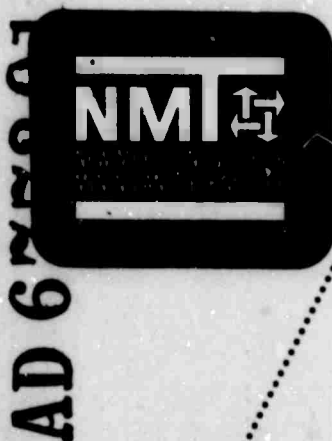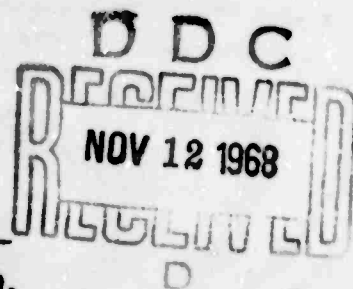
ARTIFICIAL STIMULATION OF EARTHQUAKES

ANNUAL REPORT

BY
Merle E. Hanson
Research Engineer

August 1968

NEW MEXICO INSTITUTE OF MINING AND TECHNOLOGY

Leadership in Science ··· Research and Education   Socorro, N. M. 87801

38
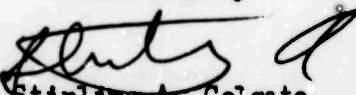
Annual Report

Artificial Stimulation Of Earthquakes

BY

Merle E. Hanson
Research Engineer

Submitted by

Stirling A. Colgate
President and Director
of Research

Contractor

New Mexico Institute of Mining and Technology, Socorro, New Mexico 87801
Tel: 505-835-5312

ANNUAL REPORT

ARTIFICIAL STIMULATION OF EARTHQUAKES

NEW MEXICO INSTITUTE OF MINING AND TECHNOLOGY

Merle Hanson

Contract No. F44 620-67-C-0113

The possibility of predictably creating artificial earthquakes through fluid infection into geologic structures is the purpose of this investigation. Seismic activity occurring in the Denver, Colorado, region which may or may not have been caused by injecting fluids into the Rocky Mountain Arsenal waste injection well has raised the question. An understanding of the phenomena was undertaken through analytic means. Obviously this work has a direct application for the objectives of underground nuclear test control.

This report contains a brief summary of the reasons why a stable two dimensional elastic dynamics numerical calculational technique had to be developed. In addition, the technique is described briefly in the general section of the report and in more detail in the appendix. The results discuss some simulations of brittle fractures propagating through an isotropic elastic media. Emphasis is placed on the fact that the simulated fractures, using simple failure criteria, propagate at speeds greater than those normally predicted in the literature. These simulations exhibit the fact that the description of dynamic fracture phenomenon is more complex than those used.

Code solution comparison with analytic solutions in seismic problems indicate that the method is sound. Further development of fracture models is required to understand the effect of high pressure fluids in creating or driving fractures in geologic strata.

A photo stress meter was purchased during the contract year to use for correlation purposes with the analytic model.

ABSTRACT

A discussion of a two dimensional elastic dynamics technique
developed to simulate seismic disturbances as a result of various
input or grid created disturbances. The method exhibits calculational
stability over other techniques using quadrilateral grids. A quieter
mesh results from which more information can be extracted from the
calculation. The results section discusses simulations of brittle
fractures propagating through the isotropic elastic media. Emphasis
is placed on the fact that the simulated cracks, using simple failure
criteria, propagate at speeds greater than normally predicted in the
literature. These simulations exhibit that the description of dynamic
failure is more complex than those used.

- A -

INTRODUCTION AND SUMMARY

This report summarizes the work performed during the first contract year in the research on Artificial Stimulation of Earthquakes, Contract No. F44620-67-C-0113, at the New Mexico Institute of Mining and Technology. Initially, the work was directed toward applying the elastic dynamics description in the existing two-dimensional Langrangian tensor hydrocodes to the seismic problems requiring solution for this analysis. These methods, when an appropriate damping was used, proved to be calculationally stable; however, the damping term was not adequate for the low-power level of disturbances calculated for the seismic problems; it tended to spread a disturbance over large areas of the grid in a nonphysical manner. To overcome this problem, equations describing a Cosserat continuum were studied, but it was not physically realistic to apply the higher order derivatives in terms of differences to the Langrangian mesh. Two alternatives evident at this time for applying the dynamic finite element technique to the seismic problem were (a) to use computers with larger active storage, permitting the calculation of more mesh intersections and thereby reducing the zone size so that the spreading of the disturbance, while affecting the same number of zones, would cover a much smaller part of the continuum or (b) to try to develop another description that would include additional constraints in the equations describing strain, thereby superseding the requirement for the damping constraints needed in some of the existing techniques. For obvious reasons, the decision was made to develop a calculational technique suitable for the simulation of seismic type of problems. This technique was developed and is described briefly in the appendix. Correlation with problems having analytic solutions has not shown serious differences between the code solutions and the analytic solutions. During the latter part of the contract year, this code has been applied to problems of hydraulically driven cracks and shear cracks. Dynamic simulations of crack phenomena using the code do not compare in crack velocity with generally accepted published results indicating that dynamic failure of isotropic elastic media is quite complicated. A literature search is in progress for information that will help provide an understanding of the cracking phenomena.

The possibility of predictably creating artificial earthquakes through fluid injection into geologic structures, is the purpose of this investigation. Earthquake activity in the Denver, Colorado, area during and after waste-fluid injection in the Rocky Mountain Arsenal injection well indicated that artificial triggering of earthquake activity by injecting high-pressure fluid into geologic strata might be possible. We do not intend to imply that the injection of fluids at the RMA well caused the seismic activity in the Denver area; however, it is certainly conceivable. An understanding of the phenomena was undertaken through analytic means by simulating stress fields dynamically with a two-dimensional, finite element technique. Although the analysis has not been completed, the approach seems sound and in addition to solutions of dynamic release of stress fields in rock needed for this task, the technique should prove valuable for other seismological studies. Obviously, this work has a direct application for underground nuclear test control, since a significant background of seismic noise created either intentionally or unintentionally could mask underground nuclear shots. In addition, small seismic disturbances could be misunderstood for underground nuclear shots or vice versa.

GENERAL

A standard method for handling two-dimensional elastic-plastic
formulations in numerical form has been published by Wilkins [1].
By his method, the strain rates within a Langrangian mesh are
calculated from the velocities and co-ordinates of the mesh points,
then integrated to obtain the strain. This method does not provide
the necessary constraints for a complete description of the strain and,
hence, the stress field. For this reason, the calculations are
absolutely unstable, so the method is sometimes stabilized by use of
what is called a rotational damping term [2]. The rotational damping
constraints are obtained by calculating pseudo pressures from the rates
of rotation of line segments on both sides of the mass point. The pseudo
pressures, which are proportional to difference of the rates of rotation
of opposing line segments of a mesh point, are then applied to oppose
the motion of the mesh point to reduce the difference in the opposing
rates of rotation. This method appears to work well where the event to
be simulated occurs in short time periods compared to the rotation or
distortion of the mesh caused by the lack of constraint in the strain
description.

This technique for constructing difference equations in Langrangian
form, when applied to seismic problems, spreads a disturbance in a non-
physical manner over large areas of the grid, making it extremely complex.
The rotational damping term, which calculates pseudo pressures of the order
of magnitude of the calculated stress level in the grid near the disturb-
ance, caused the spreading. Dimensions of the extended source were large
compared to a physically realistic detector dimension. Without the
rotational damping terms, the grid distorted nonphysically to the point
where little information could be extracted from the calculations. This
left two alternatives; either to attempt to build another formulation
where the constraints required for stability were contained in the numerical
algorithms or to attempt to use the existing formulations on larger computers,
which would allow the zoning to be sufficiently fine that the rotational
damping terms, while affecting the same number of zones, would cover only
small parts of the total mesh and would not seriously affect the results

4

of the calculation. Reduction of the zone size in the continuum
description would also reduce the calculational time step per cycle,
thereby increasing the number of cycles to be calculated for a given
problem. Increasing the number of cycles along with the greater number
of zones required to describe the continuum would make the computer
running time prohibitively long. In addition, one wants to describe the
largest continuum possible with the computer equipment available, since
a nonphysical boundary will always create reflections from incident waves
in an elastic medium. Since it is not usually possible to simulate the
complete continuum to the detail required with existing computer equip-
ment, only small sections can be considered, thereby introducing non-
physical boundaries where the section of the continuum terminates. One
might absorb the energy at the boundary from an incident wave with a
given wave number, but in a two-dimensional description of elastic media,
waves of different numbers nearly always exist. For example, consider
the irrotational and equivolume waves in a Hookean material.

Because we wanted to simulate the largest segment possible of the
continuum to obtain the most information before reflected waves from the
boundaries affect the media of interest, we directed work toward develop-
ment of a formulation that could adequately perform the calculation.
This resulted in a new two-dimensional elastic dynamics code, briefly
described in the appendix.

Correlation of this technique with problems having analytic solutions
has not shown serious differences between the code solutions and the an-
alytic solutions. The following observations have been made on a
computer simulation of Lamb's Problem (a source-detector problem on an
elastic isotropic half space):

1. P, S, and Rayleigh waves exist and were calculated at nearly
   the expected velocities.

2. A point source seems to be extended only over the zone size
   of the Langrangian mesh.

3. The calculations were stable without any damping, either tensor
   or rotational.

4. The direction of motion resulting from the P, S, and Rayleigh
    waves agrees with the expected motions.

Other observations have been made during checks and correlation
work with the code. The method calculates the correct stress per zone
in both the shear and normal cases. Dynamically, this code simulates
slightly reduced, but predicted, wave speeds. According to a stability
analysis, all finite elemental calculational techniques will show a
reduced wave speed. The amount a wave is slowed is a function of the
zone size, input disturbance rise time, and the calculational time step.
Dispersion errors can be expected if an input disturbance has a rise
time shorter than the fastest wave traversal time for a Langrangian zone.
Other checks are described in reference [3].

The computational code can handle up to 2400 mesh points on an
IBM 360 Model 44 computer. Computational speed with the code in its
present form is about 4500 zone-cycles a second on this computer.

The two-dimensional technique is now being applied to the phenomenon
of hydraulically driven fractures in brittle elastic isotropic media. In
addition, strata under high shear stress with preferred lines of failure
are being simulated. These shear-fracture patterns are being made to
help understand the phenomenon of water or other fluids lubricating an
existing fault surface under large lateral loads. The calculations made
to date are discussed later in this report and apparently do not agree
with previous analytic solutions of the same types of problems. These
differences will have to be resolved. Superposition of stress fields
along with diffusion waves in the strata can then be attempted.

6

Several calculations have been made with the code. These include simulations of both dynamic and static fractures. The stress field around a static crack (Fig. 1 and 2), which was loaded by a hydrostatic pressure within the crack, exhibits concentrations at the tip of the crack and at both sides of the tip concentrations at the sides of the tip are areas of high shear stress. The medium simulated had the Lame' constants λ and μ equal to $10''$ dynes per square centimeter and Poisson's ratio equal to 0.25. This calculation was performed with the dynamic code by forcing the dynamics to settle to a minimum energy configuration. Greater detail in the stress field can be expected with smaller zones; however, increasing the number of zones will also increase the calculational time. The calculational mesh used had 15 x 19 grid intersections. Examination of the contours indicates that the stress field and the distortion are not symmetrical, since the crack was not placed in the center of the medium. A similar calculation was performed with the crack discontinuity located symmetrically and a symmetric field was calculated. The sawtooth effect seen on both sides of the crack on the computer plot is caused by the routines that plot the contours, not by the dynamic code. Other contours that do not show a smooth appearance occur in areas where the contoured function has a shallow gradient.

Calculations of brittle cracks propagating through elastic isotropic media have been performed. A simulation of a tensile crack was made on a grid distorted for a tensile uniaxial stress field. The failure criterion chosen for crack propagation was a simple tensile break. For example, the Langrangian zone would not support any tensile stress perpendicular to the break or shear stress parallel to the break after either of the principal stresses had exceeded a certain value. Since for the tensile test, the zone would not show a crack closure, the shear stress did not have to be modified for tangential movement of the crack surface in the event that a normal force of compression existed within the zone. The uniaxial stress in the medium at the start of the calculation was static at a value of 1 kilobar. Again the Lame' constants λ and μ were $10''$ dynes/cm^2 and Poisson's ratio was 0.25. With a density of 2.7 gm/cm^3, the compressional

7

wave speed was 0.3333 cm/μ sec, and the distortional wave speed was 0.1924 cm/μ sec. The start of the crack was initiated by simulating the situation that three zones along one boundary of the grid would suddenly support neither tensile nor shear stress through the center of the zone parallel to two of the zone sides. Three runs were made with three tensile failure levels chosen, 1.3, 1.5 and 1.8 kilobars. The crack was simulated to propagate at distortional wave speed for the 1.5 kilobar tensile strength and slightly less in the case 1.8 kilobar breaking strength. For the breaking strength of 1.3 kilobars, the fracture propagated at a speed faster than the distortional wave speed. For all three runs, the crack moved straight across the grid perpendicular to the uniaxial stress field, showing no indication of branching or splaying. A plot of the elastic flow field is shown in Figure 3 for the tensile breaking strength of 1.5 kilobars.

Due to the elastic radiation patterns the energy released from tensile fracture cannot propagate forward of the crack tip at speeds greater than the distortional wave speed. The crack then should not propagate at speeds greater than this, either. The code uses a finite size element, and the beam effect of the finite calculational elements may be a factor in the high crack velocity for the smaller failure level (1.3 kilobars). In addition, dispersion could exist in the calculational technique because of too high energy release rates in the fracture model, which may also affect the fracture velocity. However, the failure phenomenon for a dynamically propagating fracture may not be so simple as the one stated. Currently, a literature search is under way to help resolve this and other problems.

As a preliminary simulation of the effect of water lubricating a sheared medium with a plane of weakness, calculations were performed with the mesh in a state of pure shear. The medium was relaxed with an imposed shear of 0.01, corresponding to 1 kilobar shear stress using the same Lame' constants and Poisson's ratio as before. In this instance, a plane of weakness was chosen laterally through the mesh; failure could occur only along this plane. This would be analogous to marking a pane of glass with a glass cutter and inducing failure along the scribed line. The failure model chosen was such that when the shear stress along this

line exceeded a certain value, shear fracture would occur and a new
shear stress would be calculated proportional to the normal force, if
compressive, but opposite, to the direction of motion. In addition,
if the relative motion across the crack approached zero, the relative
motion was stopped and a static frictional force was used for the shear
force in the zone.

Simulations on the sheared medium were performed with this failure
model. The fracture was started by removing the shear force in three
zones on one boundary of the mesh. Three calculations were made with
different failure levels in the fracture model. The levels chosen for
the parametric study were $1.3\ T^{o}_{xy}$, $1.5\ T^{o}_{xy}$, and $1.8\ T^{o}_{xy}$, where
T^{o}_{xy} is the initial shear stress in the zone. In all three calculations,
the fracture speed stabilized at approximately the compressional wave
speed. The calculated differences in the three simulations caused by
the changes in the magnitude of fracture or slip level resulted in
changing the time required to build up to this speed.

Examination of some of the literature indicates that the shear
fracture should not propagate at the compressional wave speed and that
some writers [4] propose a fracture toughness term as the fracture speed
increases. A term of the form $A\sqrt{\partial T_{xy}/\partial x}$ was included in the
fracture model to simulate the resistance to fracture as the fracture
speed increases. When this term was included, the fracture or slip
occurred when the shear stress became greater than a minimum fracture
shear and greater than the toughening term. In addition, fracture always
occurred if the shear stress became greater than some maximum level.
In equation form, fracture would occur if

$$T_{xy}^{n} > T_{min} \qquad \text{and} \qquad T_{xy}^{n} > \sqrt{\partial T_{xy}/\partial x}$$

or

$$T_{xy}^{n} > T_{max}$$

where the co-ordinate X is taken as the co-ordinate of the crack center
line and A is a constant. For this calculation A was taken as 0.08.

9

Using this fracture model, the fracture speed stabilized at about 0.83 of the compressional wave speed. This calculation showed that a more complete physical description of dynamic fracture is required. Contour plots of the shear strain indicated that it did not increase ahead of the crack tip as it had with the nonrate dependent term included in the fracture model (Fig. 4). Plots of the velocity vectors of the mass points provide a good indication of the elastic radiation patterns (Fig. 5). These patterns for shear and dilatational radiation are superimposed on the plots, but close examination will show the dilatational patterns quite clearly. A magnification of the grid plot (Fig. 6), which is actually a plot of the medium itself, evidences a twisting of the crack, along with a tendency to open slightly, near the tip. The stress field did not have a tensile stress imposed, so this opening apparently results from the dynamic crack propagation.

Other calculations included simulations of slower energy release rates from the crack opening. These studies were performed to determine if the crack was releasing energy at too fast a rate for the code to calculate properly. Since the code has to permit a crack to traverse an entire zone at the instant of failure, the energy release rate could be causing a dispersion of the energy in the calculation. These studies of slower release rates, where the fracture energy was released over a longer period of time, did not indicate that dispersion contributed to the calculated high crack velocities. The effect of slower energy release rates was, again, to slow the rate of buildup to a constant fracture speed.

All the crack propagation simulations were performed with a 30 x 60 two-dimensional mesh. The problems were set up so that the fracture would run parallel to the long side of the mesh. With the fractures centered, a reflected wave from a parallel side of the mesh could not impinge on the fracture discontinuity until 84 microseconds of problem time had elapsed.

Discussion of these fracture simulations is included in this report for completeness and to illustrate that dynamic fracture is a complex phenomenon. The failure criterion used here apparently does not describe the phenomenon of dynamic fracture.

B. Cotterell [4] states that if a crack is propagating in an infinite plane, the crack extension force will continually increase unless the crack is accelerating all the time. Experimental evidence, although not conclusive, indicates that brittle fractures in steel quickly assume a steady speed of propagation. If this is true, the fracture toughness must increase with the stress intensity. It is unlikely that such a phenomenon could continue indefinitely; at some stage, the excess energy should be absorbed by a fracture branching.

Preliminary studies of the literature indicate that, analytically, the study of moving cracks has been concentrated on two basic types: (a) a crack of constant length traversing a uniform stress field at constant velocity [5] and (b) a crack where length symmetrically increases from zero with constant velocity [4, 5]. Natural cracks are quite obviously of type (b), since type (a) assumes that the fracture is healing behind a constant-length crack.

An understanding of fracture phenomena in geologic strata has fundamental importance to the work undertaken in this contract. The indications of the analysis performed and discussed in this report show that a complete literature search is imperative and that further analysis and correlations must be made.

CONCLUSIONS

The two-dimensional elastic dynamic code developed for use in the
seismic problems produces a much quieter mesh from which more information
can be extracted than do some of the existing formulations. Correlation
with the source detector problem (Lamb's problem) on an isotropic half
space shows that the method is sound. Simulations of fluid-driven
fractures and a fluid-lubricated fault surface under lateral load indicate
that simple fracture models do not provide a complete description of the
dynamic failure phenomenon. Further development work on fracture models,
with an accompaning literature search, is required.

Difference Equations For Two-Dimensional Flow

A.G. Petschek and M.E. Hanson

ABSTRACT

An improved technique for handling two-dimensional elastic flow
is applied to several physical problems. The method differs from
older methods in that no unresisted distortions of the mesh are allowed.
A much quieter mesh results, and more information can be extracted from
the calculation.

ACKNOWLEDGMENTS

BIBLIOGRAPHY

1. M.L. Wilkins, Meth. in Comp. Physics 3, 211 (1964)

2. G. Maenchen and S.Sack, Meth in Comp. Physics 3, 181 (1964)

3. A.G. Petschek and M.E. Hanson, Difference Equations For Two-
    Dimensional Elastic Flow, to be published in J. Comp. Phys.

4. B. Cotterell, J. Appl. Mech., 31, Trans. ASME, 86, Series E, 12 (1964)

5. E.H. Yoffe, Phil. Mag., 42, Series 7, 739 (1951)

6. K.B. Broberg, Arkiv For Fysik, 18, 159 (1960)

7. J.M. Walsh, M.R. Rile, R.G. McQueen, and F.L. Yarger, Phys. Rev.,
    108 196, (1957)

APPENDIX

FINITE DIFFERENCE EQUATIONS FOR THE TWO DIMENSIONAL ELASTIC DYNAMICS CODE "TEMS"

This description is given in rectangular coordinates.

A. THE CALCULATIONAL GRID AND MASS ZONING

A two dimensional Langrangian grid is placed in the material, dividing the material into rectangles. Figure 7 is a schematic of the grid and a numbering system for the center and corners of the zones used in this description of the code. In particular

$$①= k + \frac{1}{2}, l + \frac{1}{2} \qquad 1 = k, l$$

$$②= k + \frac{1}{2}, l - \frac{1}{2} \qquad 2 = k, l + 1$$

$$③= k - \frac{1}{2}, l - \frac{1}{2} \qquad 3 = k + 1, l + 1$$

$$④= k - \frac{1}{2}, l + \frac{1}{2} \qquad 4 = k + 1, l$$

The mass at each vertex of the rectangles is calculated initially (at time zero) and held constant for the entire calculation. This ensures conservation of mass in the calculation. The mass concentrated at each vertex is taken as 1/4 the sum of the masses of the adjoining zones. For example:

$$m_{①} = \rho_{①}^{0} A_{①}^{0} \qquad (A1)$$

$$m_{k,l} = \frac{1}{4} (m_{①} + m_{②} + m_{③} + m_{④})$$

The masses at the other vertices are calculated similarly. The area of a quadrangle is taken as

$$A_1^n = (A_I)_1^n + (A_{II})_1^n$$

$$(A_I)_1^n = \frac{1}{2}\left[x_2^n(y_3^n - y_4^n) + x_3^n(y_4^n - y_2^n) + x_4^n(y_2^n - y_3^n)\right] \qquad (A2)$$

$$(A_{II})_1^n = \frac{1}{2}\left[x_2^n(y_4^n - y_1^n) + x_4^n(y_1^n - y_2^n) + x_1^n(y_2^n - y_4^n)\right]$$

A_I and A_{II} are the areas of the triangles I and II.

B. STATE EQUATIONS

The compression at cycle n is given by

$$\eta_i^{\,n} = \left[\frac{\rho^n}{\rho^0}\right]_i = \left[\frac{A^0}{A^n}\right]_i \qquad (A3)$$

The code permits the effective bulk modulus to be given by an expansion
of the form

$$K_i^n = \left[\frac{\partial \rho}{\partial \eta}\right]_i^n = a + 2b\,(\eta_i^{\,n} - 1) + 3c\,(\eta_i^{\,n} - 1)^2 + 4d\,(\eta_i^{\,n} - 1)^3 \qquad (A4)$$

where the coefficients b, c, d ... are empirical fits to experimental
shock data and can be found in the literature, for example Walsh et al.
[7]. The coefficient a is the linear bulk modulus of the material.
Given one of the Lamé constants and Poisson's ratio the remaining Lamé
constants can be found for linear elasticity. Poisson's ratio is taken
to be constant so that the Lamé "constants" are given by

$$\mu_i^{\,n} = \frac{3}{2}K_i^n\left(\frac{1 - 2\nu}{1 + \nu}\right)$$

$$\lambda_i^{\,n} = \frac{2\mu_i^{\,n}\nu}{1 - 2\nu} \qquad (A5)$$

where μ is the shear modulus and ν is Poisson's ratio.

C. STRAINS AND STRESSES

Consider a rectangle whose original corners were at (X, Y), $(X + L, Y)$, $(X + L, Y + K)$, $(X, Y + K)$ and let the corners presently be at (x, y), $(x + l_2, y + k_2)$, $(x + l_3, y + k_3)$, $(x + l_4, y + k_4)$ as shown on Figure 8.

Now consider a point whose original coordinate was $(X + U, Y + V)$ and whose present coordinate is $(x + u, y + v)$. Expand u and v as in Eq. (A25).

The coefficients a through f can be obtained by solving Eq. (A26) which gives

$$a^n = l_2/L \qquad\qquad b^n = l_4/K$$

$$d^n = k_2/L \qquad\qquad e^n = k_4/K \qquad\qquad (A6)$$

$$c^n = (l_3 - l_2 - l_4)/LK \qquad f^n = (k_3 - k_2 - k_4)/LK$$

The distortion of the grid will produce, in general, both a rotation and a distortion of each individual mesh. As the rotation will lead to strains which, by Hooke's law, Eq. (A10), produce large stresses, it is necessary to account for the rotations separately. In the distorted mesh, a line of constant V has a slope given by Eq. (A27). Rotating the distorted mesh through the angle $-\theta$ puts this line parallel to its original orientation. After rotation through this angle, the point originally at U, V is at u', v' where

$$u' = u \cos \theta + v \sin \theta \qquad\qquad (A7)$$

$$v' = v \cos \theta - u \sin \theta$$

The strains are accordingly

$$(\epsilon_{x'}^{\theta})^n = \frac{\partial(u' - U)^n}{\partial U} = (a + cV)^n \cos \theta^n + (d + fV)^n \sin \theta^n - 1$$

$$(\epsilon_{y'}^{\theta})^n = \frac{\partial(v' - V)^n}{\partial V} = (e + fU)^n \cos \theta^n - (b + cU)^n \sin \theta^n - 1 \qquad (A8)$$

$$(\gamma_{y'x'}^{\theta})^n = \frac{\partial(v' - V)^n}{\partial U} + \frac{\partial(u' - U)^n}{\partial V} = (b + cU)^n \cos \theta^n + (e + fU)^n \sin \theta^n$$

Eliminating the trigonometric functions by use of Eq. (A27) gives

$$(\epsilon_{x'}^{\theta})^n = (\sqrt{(a + cV)^2 + (d + fV)^2} - 1)^n$$

$$(\epsilon_{y'}^{\theta})^n = \left[\frac{(ae - bd) + U(af - dc) + V(ec - bf)}{\sqrt{(a + cV)^2 + (d + fV)^2}} - 1\right]^n \qquad (A9)$$

$$(\gamma_{y'x'}^{\theta})^n = \left[\frac{(b + cU)(a + cV) + (d + fV)(e + fU)}{\sqrt{(a + cV)^2 + (d + fV)^2}}\right]^n$$

using Hooke's Law, the stresses at a point along the line of constant V are

$$(\sigma_{y'y'})^n = (2\mu + \lambda)^n (\epsilon_{y'}^{\theta}) + \lambda^n (\epsilon_{x'}^{\theta})^n$$

$$\qquad (A10)$$

$$(\sigma_{y'x'})^n = \mu^n (\gamma_{y'x'}^{\theta})^n$$

Similarly a line of constant U in the distorted mesh has a slope
given by Eq. (A28). Rotating the distorted mesh through the angle
$-\phi$ puts this line parallel to its original orientation. After rotation
the point originally at U, V is at u', v' where

$$u' = u \cos \phi - v \sin \phi$$
$$v' = v \cos \phi + u \sin \phi \qquad \qquad \text{(A11)}$$

the strains are accordingly

$$(\epsilon_{x'}^{\phi})^n = \frac{\partial (u' - U)^n}{\partial U} = (a + cV)^n \cos \phi^n - (d + fV)^n \sin \phi^n - 1$$

$$(\epsilon_{y'}^{\phi})^n = \frac{\partial (v' - V)^n}{\partial V} = (e + fU)^n \cos \phi^n + (b + cU)^n \sin \phi^n - 1 \qquad \text{(A12)}$$

$$(\gamma_{x'y'}^{\phi})^n = \frac{\partial (v' - V)^n}{\partial U} + \frac{\partial (u' - U)^n}{\partial V} = (d + fV)^n \cos \phi^n$$

$$+ (a + cV)^n \sin \phi^n$$

Again eliminating the trigonometric functions with Eq. (A28) gives

$$(\epsilon_{x'}^{\phi})^n = \left[\frac{(ae - bd) + U(af - dc) + V(ec - bf)}{\sqrt{(e + fU)^2 + (b + cU)^2}} - 1 \right]^n$$

$$(\epsilon_{y'}^{\phi})^n = \left(\sqrt{(e + fU)^2 + (b + cU)^2} - 1 \right)^n \qquad \text{(A13)}$$

$$(\gamma_{x'y'}^{\phi})^n = \left[\frac{(a + cV)(b + cU) + (d + fV)(e + fU)}{\sqrt{(e + fU)^2 + (b + cU)^2}} \right]^n$$

The stresses at a point along the line $U = $ constant are

$$(\sigma_{x'x'})^n = (2\mu + \lambda)^n (\epsilon_{x'}^{\phi})^n + \lambda^n (\epsilon_{y'}^{\phi})^n$$

$$(\sigma_{x'y'})^n = \mu^n (\gamma_{x'y'}^{\phi})^n \qquad \qquad \text{(A14)}$$

---

* The angle ϕ is taken positive in the clockwise direction and the angle θ is taken positive in the counterclockwise direction.

Occasionally it has been desirable to recover the stress field in the original frame in which case the stresses in the interior of the zone are defined by

$$(\sigma_{xx})^n = (\sigma_{x'x'})^n \cos^2 \psi + (\sigma_{y'y'})^n \sin^2 \psi - 2(\tau_{x'y'})^n \sin \psi \cos \psi$$

$$(\sigma_{yy})^n = (\sigma_{y'y'})^n \cos^2 \psi + (\sigma_{x'x'})^n \sin^2 \psi + 2(\tau_{x'y'})^n \sin \psi \cos \psi$$

(A15)

where

$$\tau_{x'y'} = (\sigma_{y'x'} + \sigma_{x'y'})^n / 2$$

$$\tan \psi = (\tan \theta^n - \tan \phi^n)/2$$

(A16)

This amounts to averaging the rotation and shear stresses computed along the lines U = constant and V = constant.

D. THE MOMENTUM EQUATIONS

For the dynamics, the stresses are integrated on the quarter zones about the mass point k, l. For example, the integration is carried out along the dashed line segments about the mass point k, l in Figure 7.

We must integrate the appropriate stresses along the line $V = K/2$ over the segment $0 \le U \le L/2$ or $L/2 \le U \le L$ depending on the zone corner bordering on the mass point. Likewise the integration must be carried out for the appropriate stresses along the line $U = L/2$ over the segment $0 \le V \le K/2$ or $K/2 \le V \le K$. Either the strain definitions (A8) and (A12) or (A9) and (A13) may be used. We will use the definitions (A8) and (A12) to correspond to the form in the text of the report. The integrations in either case are trivial

$$(F_{y'y'})_i^n = \int_{x_1}^{x_2} \left[(2\mu + \lambda)\left\{ (e + fU)\cos\theta - (b + cU)\sin\theta - 1 \right\} \right.$$

$$\left. + \lambda\left\{ (a + cK/2)\cos\theta + (d + fK/2)\sin\theta - 1 \right\} \right]^n dU \qquad (A17)$$

$$(F_{y'x'})_i^n = \int_{x_1}^{x_2} \left[\mu\left\{ (b + cU)\cos\theta + (e + fU)\sin\theta \right\} \right]^n dU$$

where x_1 and x_2 are the appropriate limits either $x_1 = 0$, $x_2 = L/2$
or $x_1 = L/2$, $x_2 = L$, and

$$(F_{x'x'})_i^n = \int_{x_3}^{x_4} \left[(2\mu + \lambda)\left\{ (a + cV)\cos\phi - (d + fV)\sin\phi - 1 \right\} \right.$$

$$\left. + \lambda\left\{ (e + fL/2)\cos\phi + (b + cL/2)\sin\phi - 1 \right\} \right]^n dV \qquad (A18)$$

$$(F_{x'y'})_i^n = \int_{x_3}^{x_4} \left[\mu\left\{ (d + fV)\cos\phi + (a + cV)\sin\phi \right\} \right]^n dV$$

where $x_3 = 0$, $x_4 = K/2$ or $x_3 = K/2$, $x_4 = K$ depending on the position
of the zone about the mass point. Then

$$(F_{y'y'})_i^n = (2\mu + \lambda)_i^n \left[(e + \alpha fL/4)\cos\theta - (b + \alpha cL/4)\sin\theta - 1 \right]_i^n L/2$$

$$+ \lambda_i^n \left[(a + cK/2)\cos\theta + (d + fK/2)\sin\theta - 1 \right]_i^n L/2 \qquad (A19)$$

$$(F_{y'x'})_i^n = \mu_i^n \left[(b + \alpha cL/4)\cos\theta + (e + \alpha fL/4)\sin\theta \right]_i^n L/2$$

and

$$(F_{x'x'})_i^n = (2\mu + \lambda)_i^n \left[(a + a\,cK/4)\cos\phi - (d + a\,fK/4)\sin\phi - 1\right]_i^n K/2$$

$$+ \lambda_i^n \left[(e + fL/2)\cos\phi + (b + cL/2)\sin\phi - 1\right]_i^n K/2 \qquad (A20)$$

$$(F_{x'y'})_i^n = \mu_i^n \left[(d + a\,fK/4)\cos\phi + (a + a\,cK/4)\sin\phi\right]_i^n K/2$$

where the subscripts i denote the zone centers, for example those numbers enclosed in circles in Figure 7, in relation to mass point k, l , and n is the cycle number.

$\quad a = 1$ for Equations (A19) for zones ① and ④
$\quad a = 1$ for Equations (A20) for zones ① and ②
$\quad a = 3$ for Equations (A19) for zones ② and ③
$\quad a = 3$ for Equations (A20) for zones ③ and ④

As in the text, the first subscript designates the normal to the surface across which a stress in the direction of the second subscript is exerted. The primes on the subscripts denote that we are in a frame rotated with respect to the original frame.

We must then rotate these forces back to the original frame to apply them to the momentum equation.

$$(F_{y'x})_i^n = (F_{y'x'})_i^n \cos\theta^n - (F_{y'y'})_i^n \sin\theta^n$$

$$\qquad (A21)$$

$$(F_{y'y})_i^n = (F_{y'y'})_i^n \cos\theta^n + (F_{y'x'})_i^n \sin\theta^n$$

and

$$(F_{x'x})_i^n = (F_{x'x'})_i^n \cos \phi^n + (F_{x'y'})_i^n \sin \phi^n$$

(A22)

$$(F_{x'y})_i^n = (F_{x'y'})_i^n \cos \phi^n - (F_{x'x'})_i^n \sin \phi^n$$

The velocities can be computed from the force field by

$$\dot{x}_{k,l}^{n+1/2} = \dot{x}_{k,l}^{n-1/2} + \left[(F_{x'x})_① - (F_{x'x})_② - (F_{x'x})_③ + (F_{x'x})_④ \right.$$

$$\left. + (F_{y'x})_① + (F_{y'x})_② - (F_{y'x})_③ - (F_{y'x})_④ \right]^n \Delta t^n / m_{k,l}$$

(A23)

$$\dot{y}_{k,l}^{n+1/2} = \dot{y}_{k,l}^{n-1/2} + \left[(F_{y'y})_① + (F_{y'y})_② - (F_{y'y})_③ - (F_{y'y})_④ \right.$$

$$\left. + (F_{x'y})_① - (F_{x'y})_② - (F_{x'y})_③ + (F_{x'y})_④ \right]^n \Delta t^n / m_{k,l}$$

The positions can be incremented by

$$x_{k,l}^{n+1} = x_{k,l}^n + \dot{x}_{k,l}^{n+1/2} \Delta t^{n+1/2}$$

(A24)

$$y_{k,l}^{n+1} = y_{k,l}^n + \dot{y}_{k,l}^{n+1/2} \Delta t^{n+1/2}$$

E. TIME STEP

In accord with the Courant criterion, the time step is taken to be the minimum over the mesh of

$$\Delta t^{n + 1/2} = C \Delta r^{n + 1}/a$$

where

$$\Delta r^{n + 1} = A^{n + 1}/S,$$

S is the longest diagonal of the quadrangle, a is the local dilitational wave speed and C has been taken to be 0.6.

F. THE MAPPING TECHNIQUE

Evidently, one ought to difference the equations so that there are no unresisted distortions of the mesh. This has been done as follows: consider a quadrilateral which was originally rectangular and had its lower left hand corner at X, Y. Let the lower left hand corner now be displaced to x, y and the point originally at X + U, Y + V be displaced to x + u, y + v. Expand the present position as a function of the original position as follows

$$u = aU + bV + cUV + \ldots$$
$$v + dU + eV + fUV + \ldots$$

(A25)

Just six parameters in the expansion have been written down because this is enough to specify completely the positions of the corners and is as many as can be determined by those positions. The term proportional to UV is preferable to one proportional to U^2 or V^2 because it maps the edges of the original rectangle into straight lines and this ensures that the meshes of the distorted lattice fit together without gaps or overlap.

The coefficients a through f may be found from the coordinates of the grid. That is, if the intersections of grid lines around the mesh are numbered from 1 to 4 as before, the one with U = V = 0 is numbered 1, and the original rectangle had the dimensions L by K, then a through f are found from

$$u_2 = aL$$

$$v_2 = dL$$

$$u_3 = aL + bK + cKL$$

$$v_3 = dL + eK + fKL \tag{A26}$$

$$u_4 = bK$$

$$v_4 = eK$$

Given a through f , one may compute the displacments u - U and v - V and from the displacements the strains as a function of position throughout the mesh.

To compute accelerations, the mesh is bisected in the X and Y directions, and the masses of the four adjacent quarter zones as associated with each mesh point. The force is computed by integrating the stress around the circumference of the mass. To do this the stresses on the line segments U = L/2, O<V<K/2; U = L/2, K/2<V<K and so forth are required. These can easily be computed from the strains, provided proper account is taken of the rotation of the mesh. To do the latter, we rotated the zone until the line along which the stress was to be computed, i. e. V = K/2 or U = L/2 was parallel to its original direction, i. e. the X or Y axis. This implies a rotation through an angle

$$\theta = \tan^{-1} \frac{d + fK/2}{a + cK/2} \tag{A27}$$

in the former case and an angle

$$\phi = \tan^{-1} \frac{b + cL/2}{e + fL/2} \tag{A28}$$

in the latter. If the rotations are not taken into account, Hooke's law as used below will give rise to large fictitious stresses.

After rotation the strain in the x direction along the line of constant V is

$$\epsilon_{x'}^{\theta} = (a + \frac{1}{2} cK) \cos \theta + (d + \frac{1}{2} fK) \sin \theta - 1. \qquad (A29)$$

The primes indicate that a rotated coordinate system is in use.

The stresses are, in the case of plane strain (no distortion perpendicular to the plane considered) by Hooke's law, for instance

$$\sigma_{y'y'} = (2\mu + \lambda) \left[(e + fU) \cos \theta - (b + cU) \sin \theta - 1 \right] +$$
$$\lambda \left[(a + \frac{1}{2} cK) \cos \theta + (d + \frac{1}{2} fK) \sin \theta - 1 \right] \qquad (A30)$$

Where μ and λ are Lamé constants and the first subscript designates the normal to the surface across which a stress in the direction of the second subscript is exerted.

The corresponding forces are obtained by integrating along the appropriate half bisector of the mesh to give, for instance

$$F_{y'y'} = \int dU \quad \sigma_{y'y'} = (2\mu + \lambda) \left[(e + \frac{1}{4} f\alpha L) \cos \theta - (b + \frac{1}{4} f\alpha L) \sin \theta - 1 \right] \frac{1}{2} L$$
$$+ \lambda \left[(a + \frac{1}{2} cK) \cos \theta + (d + \frac{1}{2} fK) \sin \theta - 1 \right] \frac{1}{2} L \qquad (A31)$$

where the limits on the integral are 0 and L/2 or L/2 and L, and α is 1 in the former case and 3 in the latter. Then the force is rotated back into the original Eulerian frame, that is

$$F_{y'y} = F_{y'y'} \cos \theta + F_{y'x'} \sin \theta$$
$$F_{y'x} = F_{y'y'} \sin \theta + F_{y'x'} \cos \theta \qquad (A32)$$

Finally the force is summed over the eight line segments surrounding the intersection, and is used to accelerate the mass centered there.

G. GENERAL

The boundaries of the mesh can be treated as having phantom zones with no tractions, normal forces or masses. The code will not correctly calculate displacement disturbances with frequencies shorter than the time acquired for a dilatational disturbance to cross 4 zones. If these disturbances are produced on the boundaries of the mesh, dispersion of the induced wave trains is observed.

A tensor viscosity has been developed and used with the code.
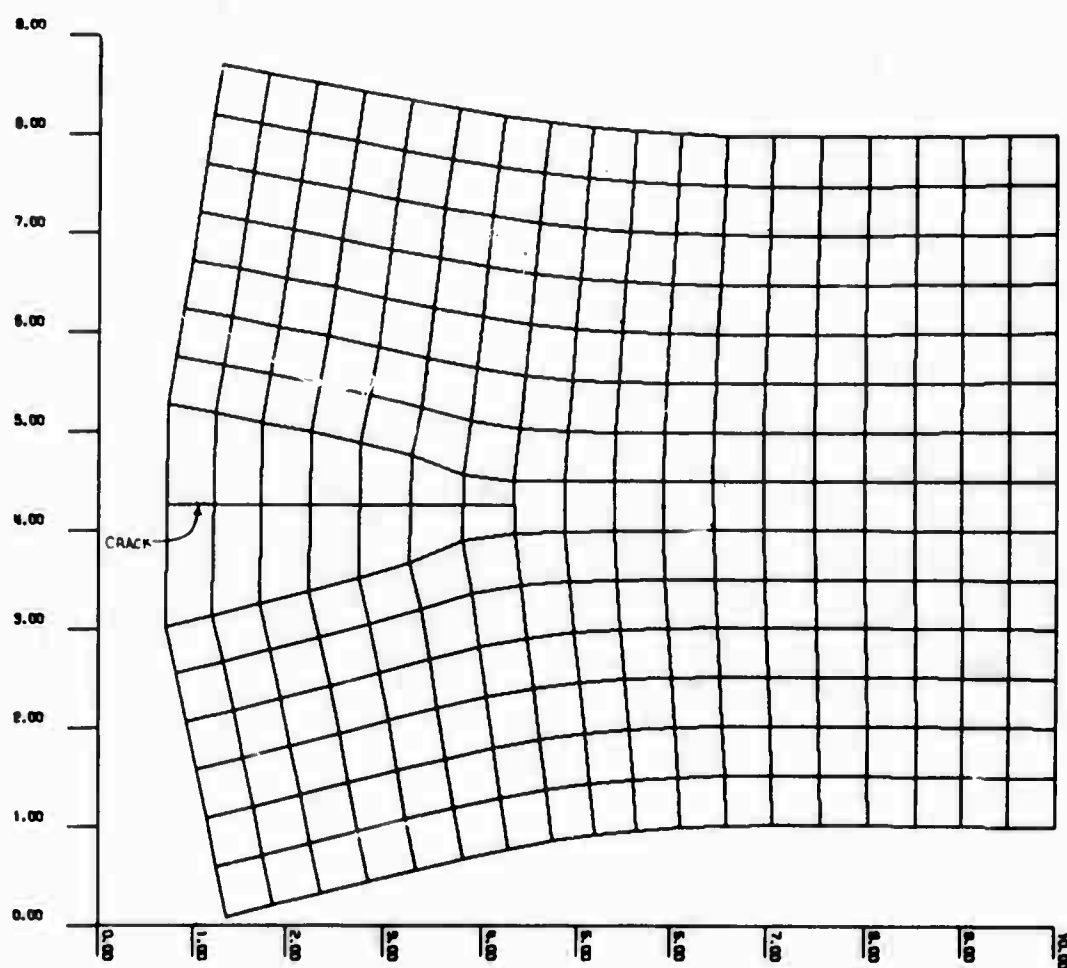
Figure 1 Grid for static crack with distortion magnified by 10. Hydrostatic pressure
in the crack was taken as 1 kilobar, Lame' constants for media were
$\lambda = \mu = 0.1$ megabars.
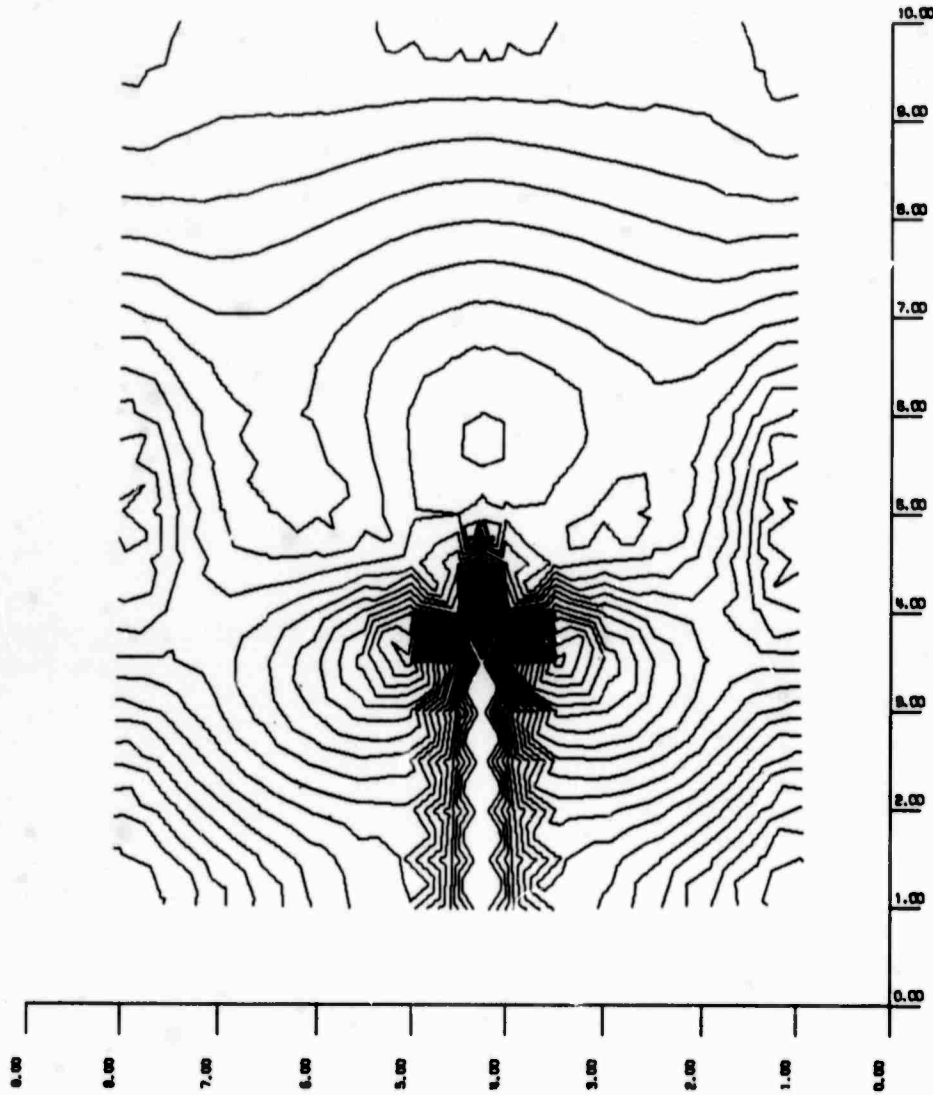
Figure 2 Contours of P-Q for the internally loaded static crack, where P and Q are the principal stresses. Contour interval is 125 bars, minimum contour is 125 bars, maximum contour is 3500 bars, the sawtooth affect on both sides of the crack is due to the plotting routines. No initial load was imposed on the medium. Contours are of the grid shown on figure 1.
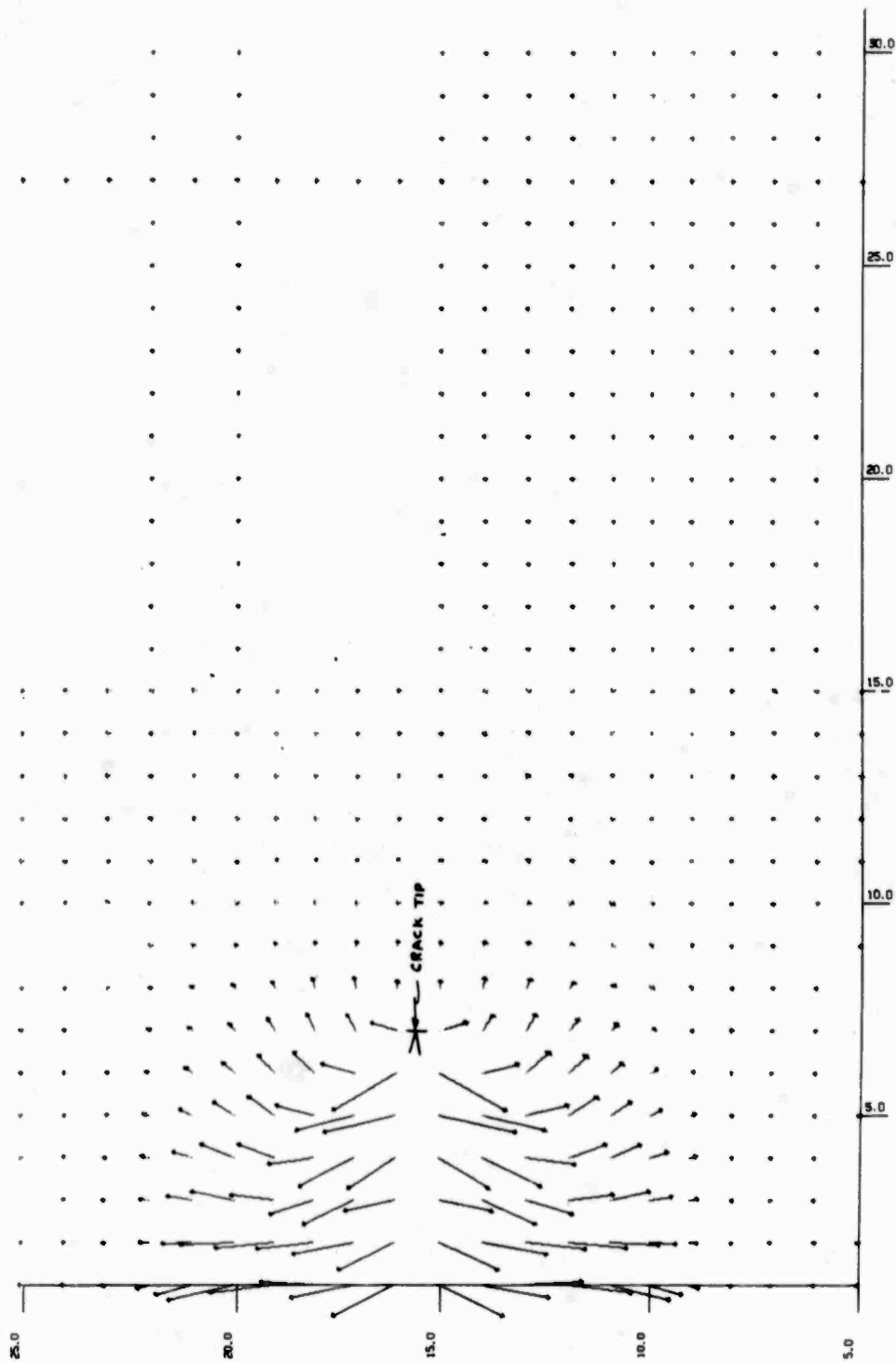
Figure 3   Vector velocity plot of mass points or elastic flow field around tensile crack in a uniaxial strained media. Time slice of plot is 28.8 μ sec after crack was initiated. Vector length magnification is 625. Zone size for calculation was 1 centimeter square. Lame' constants for the media were $\lambda = \mu = 0.1$ megabars.
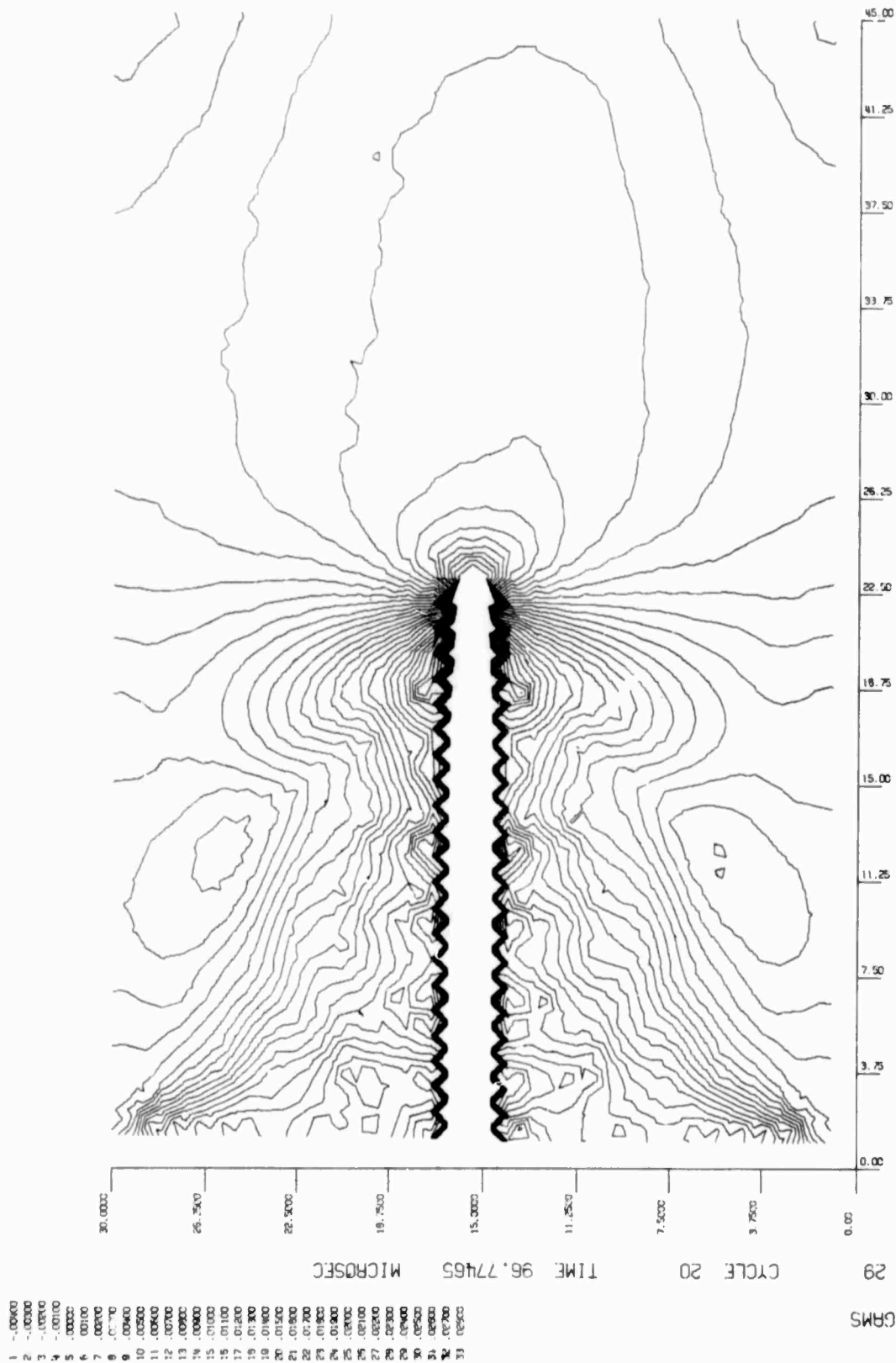
Figure 4 Contours of the shearing strain for the shear or slip fracture. The shear
failure model included the toughening term described in the report.
Contour interval is .001, minimum contour is -.004, maximum contour is
.028. Sawtooth effect on both sides of the crack is caused by the plotting
routines. Time of plot is 96.7 μ sec after crack was initiated. Lame'
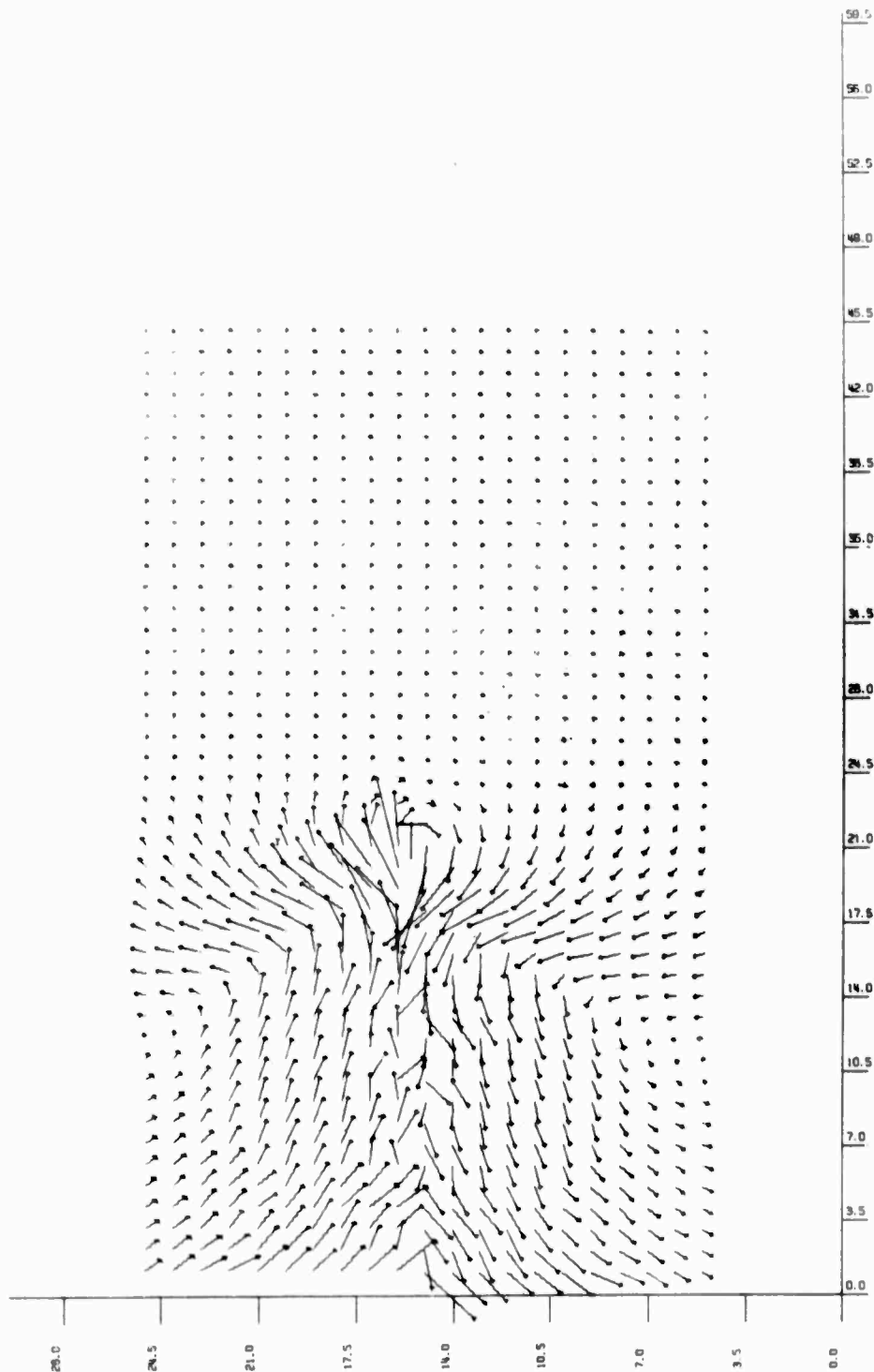constants for the media were λ = μ = 0.1 megabars.

Figure 5 Velocity vector plot or elastic flow field around the shear fracture in the media under pure shear when crack was initiated. Time slice was 94.4 µ seconds after crack was initiated. Fracture model contained toughening term described in the report. Vector length magnification is 250. Lame' constants for the media were λ = µ = 0.1 megabars
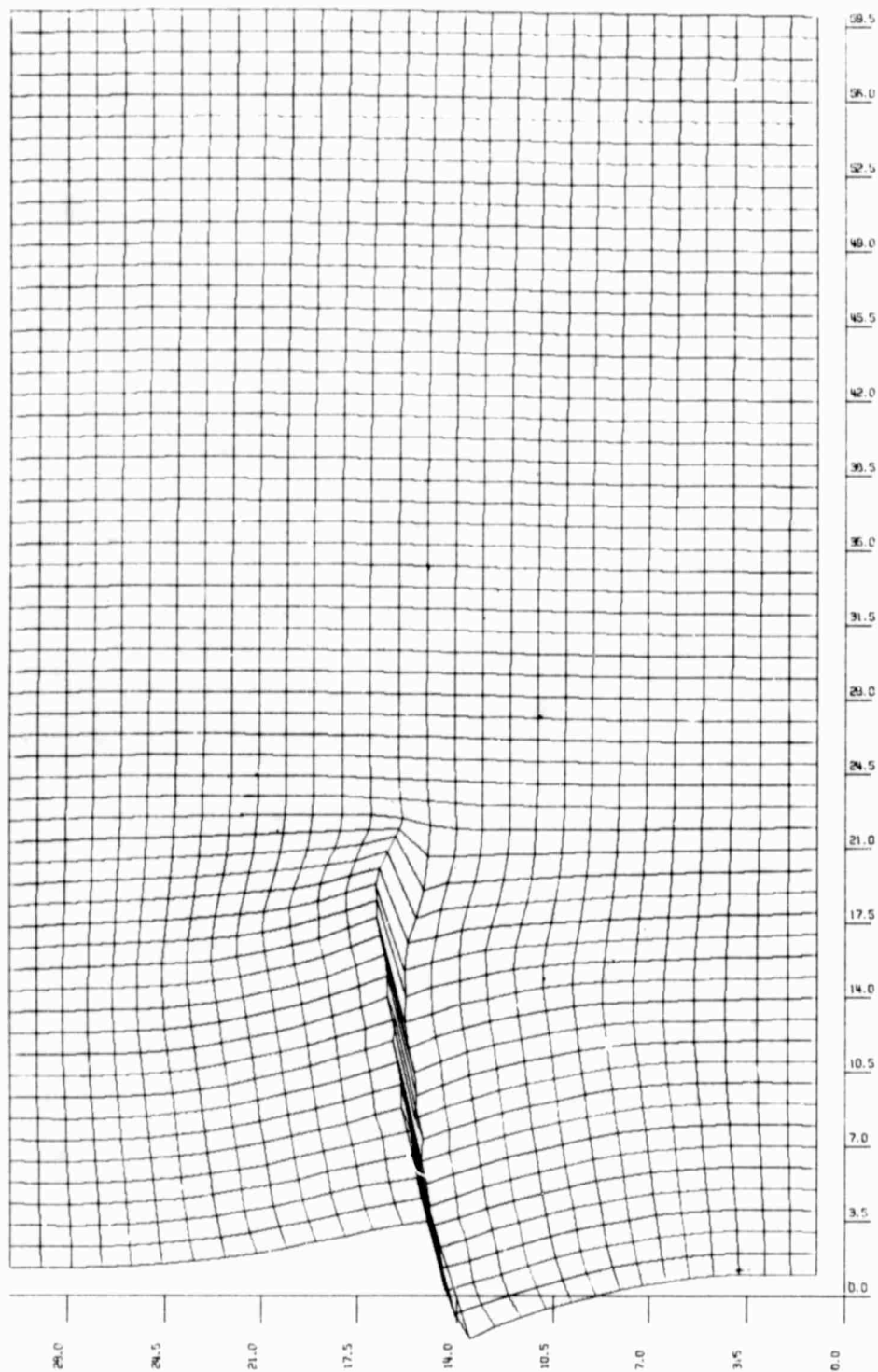
Figure 6 Grid plot of media during shear fracture in the media under pure shear. Time slice was 94.4 μ seconds after crack was initiated. All distortions were magnified by 50. Note twisting effect at crack tip.
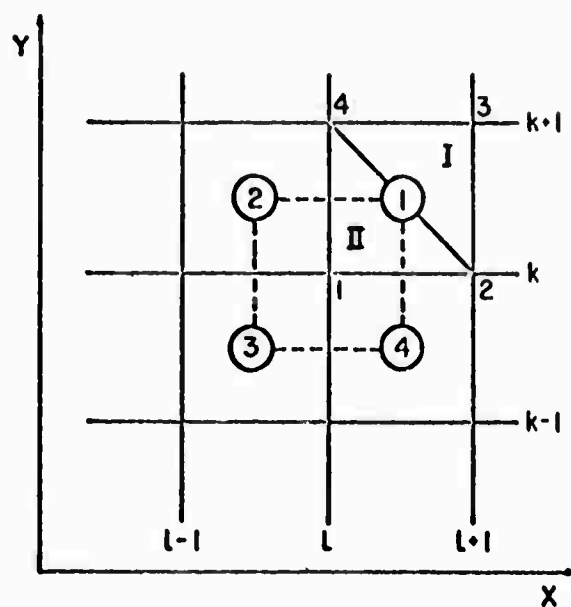
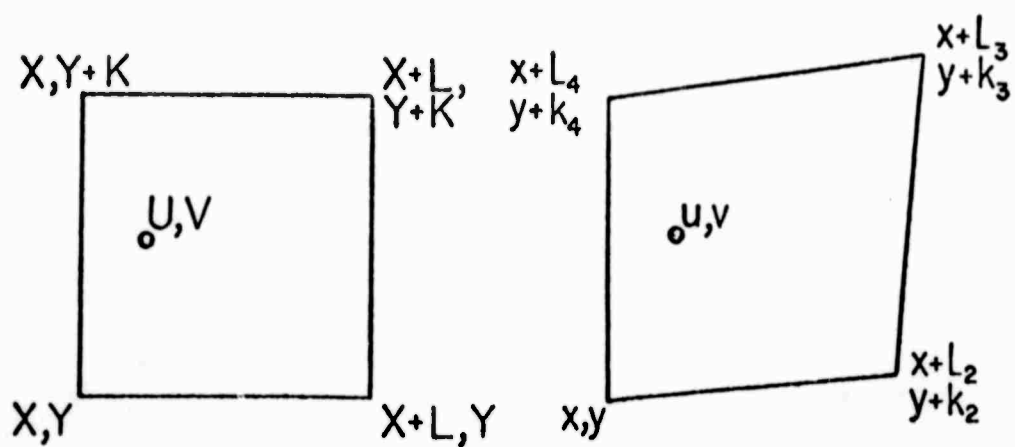Figure 7. The grid and numbering scheme for the difference equations.

Figure 8. Comparison of undistorted and distorted meshes indicating the meaning of u and v.